Electronic Supplementary Material (ESI) for Journal of Materials Chemistry A.
This journal is © The Royal Society of Chemistry 2023

Supporting Information

Tunable Hydrogen Evolution Activity by Modulating Polarization States of Ferroelectric $BaTiO_3$

Haifa Qiu,[a,b] Tong Yang,[a] Jun Zhou,[c] Ke Yang,[a] Yiran Ying,[a,b] Keda Ding,[a] Ming Yang*[a] and Haitao Huang*[a,b]

[a]Department of Applied Physics, Hong Kong Polytechnic University, Hong Kong SAR, China

[b]Research Institute for Smart Energy, The Hong Kong Polytechnic University, Hung Hom, Kowloon, Hong Kong, China.

[c]Institute of Materials Research & Engineering, A*STAR (Agency for Science, Technology and Research), 2 Fusionopolis Way, Innovis, Singapore 138634, Singapore.

*E-mail: aphhuang@polyu.edu.hk; kevin.m.yang@polyu.edu.hk

Computational details

First-principles calculations were performed using Vienna Ab-initio Simulation Package (VASP.5.4.4).[1] Unless otherwise specified, the generalized gradient approximation (GGA) with the Perdew−Burke−Ernzerhof (PBE) functional was employed to describe the exchange-correlation effects, with ionic potentials treated by projector augmented wave (PAW) approximation.[2–4] A cut-off energy of 520 eV was used in all calculations, together with electronic energy threshold of 10^{-5} eV and force criteria of 0.015 eV/ Å to achieve convergence. The dispersion correction for van der Waals interaction between absorbates and the substrates was adopted by using DFT-D3 method from Grimme et al.[5] Prior to surface calculations, bulk BTO with tetragonal structure bulk was relaxed. Both BTO (001) and (010) surfaces were modeled using 2 × 2 slabs with three Pt layers as electron reservoir. Apart from the Pt layers, the TiO_2-terminated slabs contain 11 atomic layers. The Pt layers were relaxed before they were fixed upon adsorption of hydrogen. An 8 × 8 × 8 and 4 × 4 × 1 Monkhorst-Pack *k*-point meshes were used for the integration in the Brillouin zone for BTO bulk and slab supercells, respectively.[6] A vacuum layer with the thickness of 15 Å was applied for all slabs to avoid spurious interactions. Dipole correction was considered throughout the slab calculations. The polarization of BTO bulk and slab was calculated based on the Berry phase method.[7] Apart from considering the polarization change from counterpart electronic redistribution in the slab, the slab BTO was treated as supercell only consisting of oxide atomic layers, excluding the bottom TiO_2 layer for stoichiometry sake, when calculating polarization by the method reported.[8–9] To appropriately describe the strong correlation between *d* electrons, on-site Coulomb repulsion U (U_{eff} = 6 eV) for the Ti 3*d* electrons was included to evaluate the electronic structure based on Dudarev method.[10]

The reaction equations involved in HER are given as follows:

$$^{*} + H^{+} + e^{-} \leftrightarrow H^{*} \quad \text{(Volmer step)} \tag{1}$$

$$H^{*} + H^{+} + e^{-} \leftrightarrow {}^{*} + H_2 \quad \text{(Heyrovsky step)} \tag{2}$$

$$H^{*} + H^{*} \leftrightarrow 2\,{}^{*} + H_2 \quad \text{(Tafel step)} \tag{3}$$

where * denotes the surface catalytic site and *H denotes the H atom adsorbed on the surface catalytic site. Since the formation of gaseous hydrogen ($2H^{+} + 2e^{-} \leftrightarrow H_2$) is at equilibrium state at standard condition (1atm, 298.15 K), the free energy of proton and

electron, $G(H^+ + e^-)$, can be simplified by $\frac{1}{2}G(H_2)$ based on the computational hydrogen model.[11,12] Thus, the free energy change of hydrogen adsorption for Volmer step can be derived as:

$$\Delta G_{H^*} = G_{H^*} - G_* - \frac{1}{2}G(H_2) + \Delta G(pH) \quad (4)$$

where $\Delta G(pH) = -RTln[H^+] = 0.059 \times pH$ is used to describe the pH effect from solvation.[13]

Likewise, the free energy change of hydrogen desorption for Heyrovsky:

$$\Delta G_{H_2} = G_* + \frac{1}{2}G(H_2) - G_{H^*} + \Delta G(pH) \quad (5)$$

or for Tafel step:

$$\Delta G_{H_2} = 2 \times (G_* + \frac{1}{2}G(H_2) - G_{H^*}) \quad (6)$$

The HER activity of BTO under different polarization state is mainly described by the Gibbs free energy change of hydrogen adsorption, while hydrogen adsorption strength is described by hydrogen adsorption energy. The hydrogen coverage is defined by the number of adsorbed hydrogen, n_H, over the total number of specific adsorption sites(oxygen), n_{tot}, on the studied BTO surface on which the adsorption occurs. The adsorption energy of hydrogen (ΔE_{ads}) was calculated based on[14]

$$\Delta E_{ads} = \frac{1}{n_H}(E_{BTO+nH} - E_{BTO} - \frac{n_H}{2}E_{H_2}), \quad (7)$$

where E_{BTO+nH} and E_{BTO} are the energy of the hydrogen-adsorbed final configuration and the hydrogen-free initial configuration, respectively. The Gibbs free energy change is expressed with respect to the adsorption energy by

$$\Delta G_{H^*} = \Delta E_{ads} + \frac{1}{n_H}(\Delta E_{ZPE} - T\Delta S_H), \quad (8)$$

where $\Delta E_{ZPE} = E_{ZPE}^{n_H} - \frac{n_H}{2}E_{ZPE}^{H_2}$ and $\Delta S_H = S_{n_H}^{\circ} - \frac{n_H}{2}S_{H_2}^{\circ}$ are the change in the zero point energy (ZPE) and entropy between the adsorbed state H^* and the gas phase H_2, respectively. Gibbs free energy correction was made by using VASPKIT.[15]

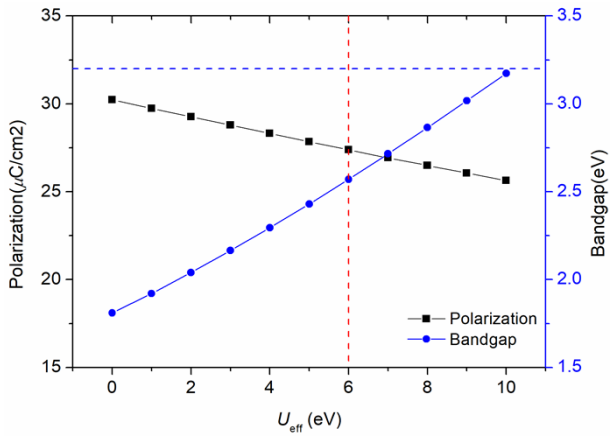

Figure S1 The evolution of polarization and bandgap with U_{eff} for bulk BTO. The blue dashed line refers to the experimental bandgap of 3.2eV.

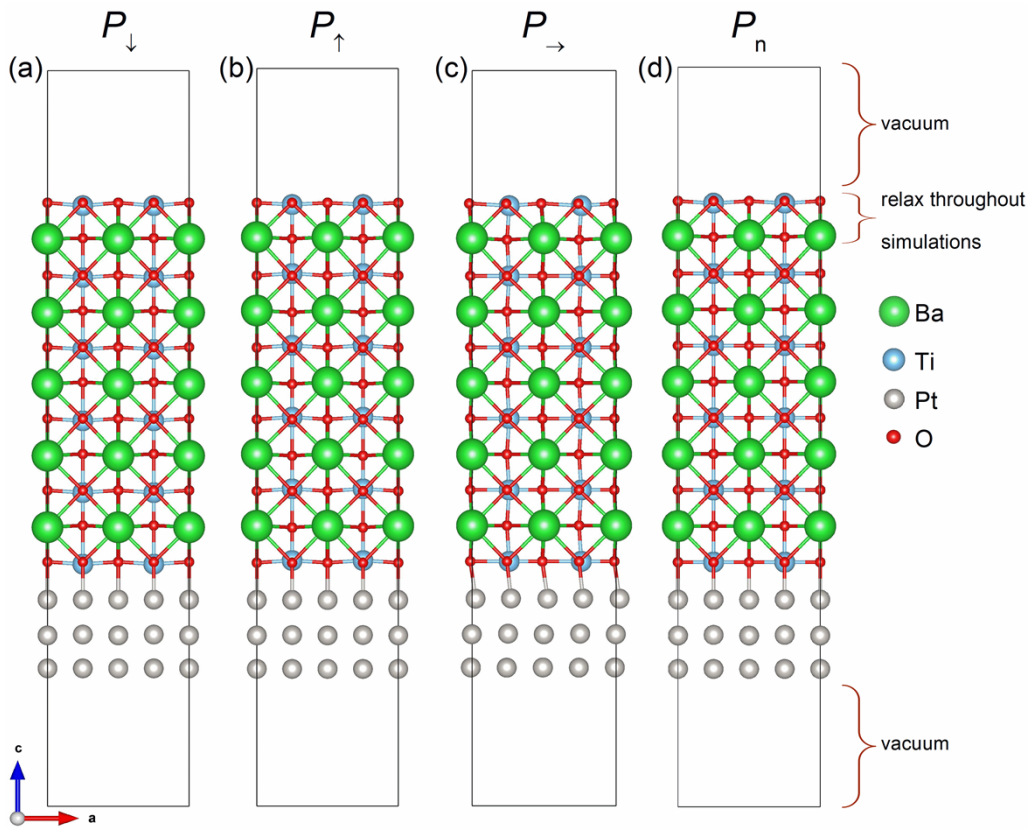

Figure S2 The sideview of whole BTO slab model after surface relaxation under varied polarization state: (a) the downward polarization state, (b) upward polarization state, (c) the rightward in-plane polarization state, and (d) the non-polar state. The three layers of platinum atoms are introduced at the bottom of the BTO slab model in order to passivate the dangling bonds of the lower BTO surface and act as an electron reservoir.

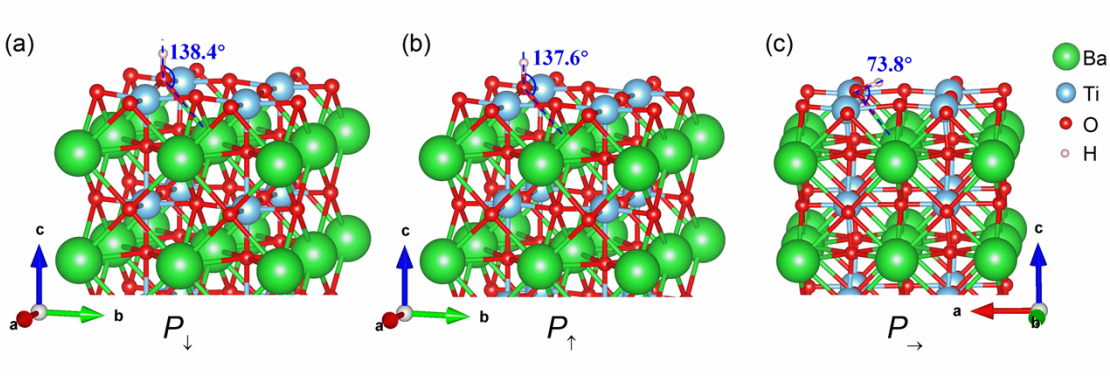

Figure S3 The Ba-O-H angle between OH dipole and neighboring Ba-O bond under various polarization states. Herein, only upper four atomic layers of BTO slabs are shown for simplicity.

Table S1 The Gibbs free energy change of hydrogen adsorption and hydrogen adsorption energy on BTO with topmost two layers relaxed under various polarization states.

Polarization state	Initial hydrogen adsorption configuration	ΔG_{H^*} /eV	E_{ads}/eV	Final hydrogen adsorption configuration	
$P_{\downarrow}$	1-Ti-Top	2.7366	2.6472	1-Ti-Top	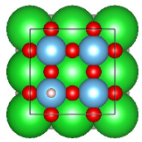
	2-O-Top	-1.4939	-1.7936	2-O-Top	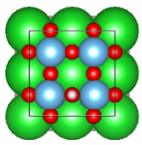
	3-Ti-O-bri	**-1.5640**	**-1.8638**	**2-O-Top**	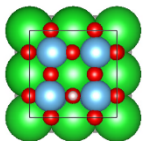
	4-hollow	0.6491	0.5507	4-hollow	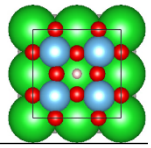
$P_{\uparrow}$	1-Ti-Top	0.8575	0.6774	1-Ti-top	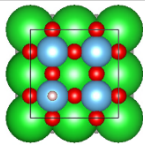
	2-O-Top	**0.2820**	**-0.0167**	**2-O-top**	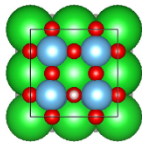
	3-Ti-O-bri	0.6288	0.4481	1-Ti-quasi-top	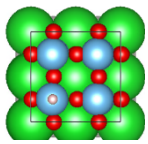

	4-hollow	0.4513	0.2702	1-Ti-quasi-top	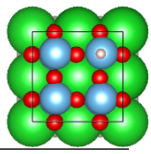
$P_{\rightarrow}$	1-Ti-Top	2.3597	2.2153	Ti-quasi-top	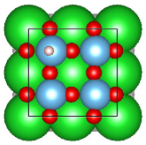
	2-O(high)-Top	0.2118	-0.0880	O-quasi-top	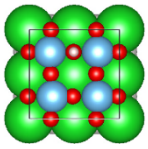
	3-Ti-O(low)-bri	**-0.2208**	**-0.5525**	**O(low)-hollow-left**	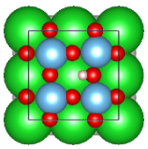
	4-hollow	-0.2082	-0.5403	O(low)-hollow-left	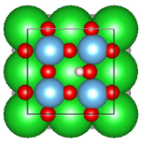
	5-O(low)-Top	-0.1927	-0.5249	O(low)-hollow-left	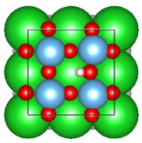
	6-Ti-O(high)-bri-left	0.2115	-0.0882	O-quasi-top	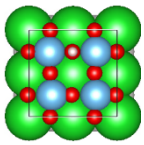
	7*L-O(low)-hollow*	-0.2082	-0.5403	O(low)-hollow-left	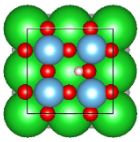
	7*R-O(low)-hollow*	-0.0392	-0.3715	O(low)-hollow-right	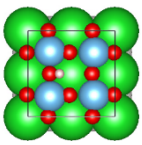
	8*U-O(high)-hollow*	-0.1974	-0.5290	O(high)-hollow-upside	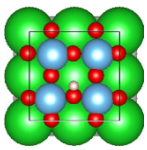
	8*D-O(high)-hollow*	-0.1969	-0.5288	O(high)-hollow-downside	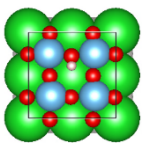
	9-Ti-O(high)-bri-right	0.2124	-0.0876	O-quasi-top	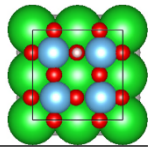

P_n	1-Ti-Top	2.3230	2.1471	1-Ti-Top	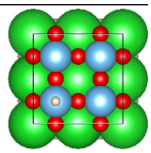
	2-O-Top	-0.0023	-0.3020	2-O-Top	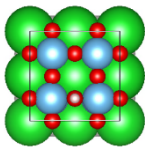
	3-Ti-O-bri	**-0.0780**	**-0.3776**	**2-O-Top**	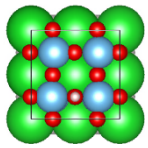
	4-hollow	2.11	2.0106	4-hollow	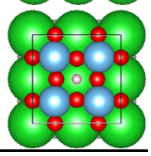

L, *R*, *U*, *D* refers to left, right, upside, downside, respectively. The initial adsorption sites 1, 2, 3, 4, …, 9 are indicated in Fig. 3a. The most stable configuration and corresponding energy values are indicated in bold fonts.

Table S2 A comparison of structural and electronic properties and free energies for the case in presence of surface reconstruction (***P***) and the one in absence (denoted as $\boldsymbol{P_0}$) under varied polarization states. (Partial data are extracted from **Figure 2**)

BTO	Surface/subsurface Rumpling (%)	Surface expansion/ Contraction (%)	Vertical polarization change[a](μC/m^2)	ΔG_{H*} /eV	$\Delta(\Delta G_{H*})^a$ /eV
***P*↓**	-132 / -4	+0.97	+6.2 (+23%)	-1.56	-0.90
***P*↑**	-59 / +93	-1.22	-3.8 (-14%)	0.28	-0.08
***P*→**	-93, -101 / +81	+0.34	+3.1(+11%)	-0.22	-1.05
$\boldsymbol{P_0}$**↓**	-100 / -100	0	0	-0.66	0
$\boldsymbol{P_0}$**↑**	+100 / +100	0	0	0.36	0
$\boldsymbol{P_0}$**→**	+100 / +100	0	0	0.83	0

[a] change in ΔG_{H*} relative to the case in absence of surface reconstruction.

We compare the Gibbs free energy changes (**Table S3**) using different damping functions in the DFT-D3 method. The results show that the HER activity trend is unaffected by the damping functions and the Gibbs free energy changes are quite

comparable, which is also a reflection of the reliability of the DFT-D3 method.

Table S3 Gibbs free energy changes of hydrogen adsorption (ΔG_{H*}) of BTO under varied polarization states using different damping functions in the DFT-D3 method.

BTO	DFT-D3(0)[a]	DFT-D3(BJ)[b]
***P*↓**	-1.56 eV	-1.49 eV
***P*↑**	+0.28 eV	+0.28 eV
***P*→**	-0.22 eV	-0.19 eV

[a] method of Grimme with zero-damping function

[b] method with Becke-Johnson damping function

Evaluation of BTO stability for HER

The catalytic stability is an important figure of merit for a good catalyst in experiments, especially for commercial applications.[17] Aqueous stability or electrochemical stability can often be reflected from the Pourbaix Diagram, where the stability is judged from thermodynamics and is computationally affordable.[18,19] So, to evaluate the electrochemical stability of polarized $BaTiO_3$, we constructed its Pourbaix phase diagram via pymatgen,[20] as shown in Figure S4.

According to the Pourbaix phase diagram, for the tetragonal BTO phase with out-of-plane polarization, the TiO_2-terminated surface should be more electrochemically stable than BaO-terminated one throughout the *E*-pH space for HER. On the contrary, BaO surface tends to be dissolved into electrolyte in the form of Ba^{2+} and $BaOH^{+}$ in acid and strongly alkaline environment, respectively, implying electrochemical instability. The results are comparable with those reported by Nongnuch Artrith.[21] For the BTO phase

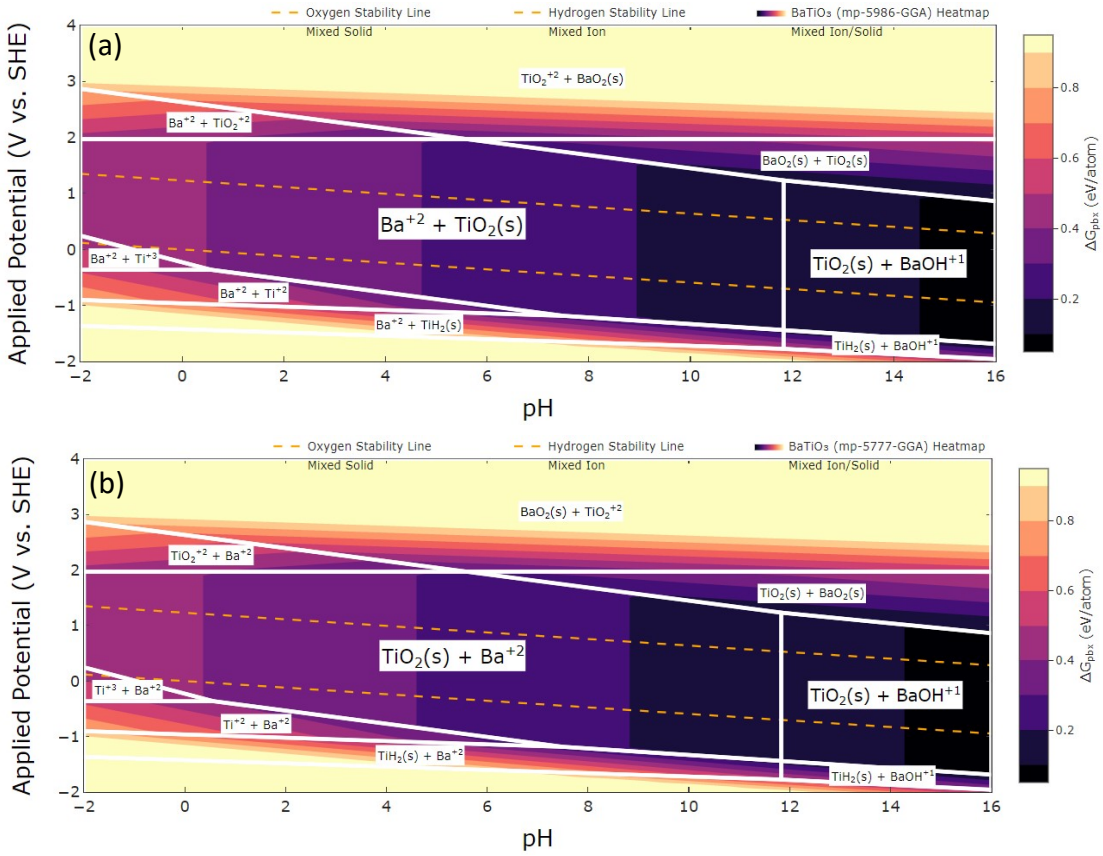

Figure S4 Pourbaix phase diagram of BTO with (a) out-of-plane polarization and (b) in-plane polarization.

with in-plane polarization, the Pourbaix phase diagram remain almost the same as shown in Figure S5b.

In addition, we also evaluated the formation energy of surface Ti vacancy on BTO surface in presence of hydrogen adsorption to simulate the dissolution of Ti into electrolyte during catalysis, which is possible as shown in the region below hydrogen stability as shown in Figure S5 below. The vacancy formation energy is calculated according to the following equation:[22]

$$E_f[X^q] = E_{tot}^{defect}[X,q] - E_{tot}^{perfect} - \sum n_i u_i - q[E_F + E_V + \Delta V]$$

where $E_{tot}^{defect}[X,q]$ is the total energy of the TiO_2-terminated BTO surface slab with Ti defect in the supercell, $E_{tot}^{perfect}$ is the total energy of the perfect TiO_2-terminated BTO surface slab, n_i denotes the total number of atoms of element i (for native host atoms Ti removed from (n_i <0) or for foreign impurity atom added to (n_i >0) in the slab model), and u_i refers to the chemical potential of element i. The value of u_{Ti} is the energy of an individual Ti atom. E_F is the Fermi level with respect to the valence band maximum

(VBM) (E_V), and ΔV is the necessary correction for aligning the electrostatic potentials between the perfect surface and a surface with defects in a charged state. Herein, for simplicity, we mainly deal with the defective TiO_2-terminated BTO surface in a neutral charge state, thus the final term in the above equation will be zero and the equation is simplified as:

$$E_f[\mathrm{Ti}] = E_{tot}^{defect}[\mathrm{Ti}] - E_{tot}^{perfect} + u_{\mathrm{Ti}}$$

In general, the more negative the formation energy value, the easier the formation process of vacancy with lower energy barrier. As shown in Figure S6, we find that the formation energy values under varied polarization state are all positive. This implies that it requires considerable energy barrier for Ti vacancy to form on BTO surface upon hydrogen adsorption, suggesting the thermodynamical surface stability of the TiO_2-terminated BTO surface in presence of hydrogen adsorption. It is noted that the BTO surface with upward and in-plane polarization shows higher formation energy value of Ti vacancy than that with downward polarization, indicating that the former polarization states could be more energetically stable during hydrogen adsorption. Therefore, the TiO_2-terminated surface in varied polarization states we choose in our study is assumed to ensure the electrochemical surface stability and long-term stability for HER, regardless of the polarization states involved.

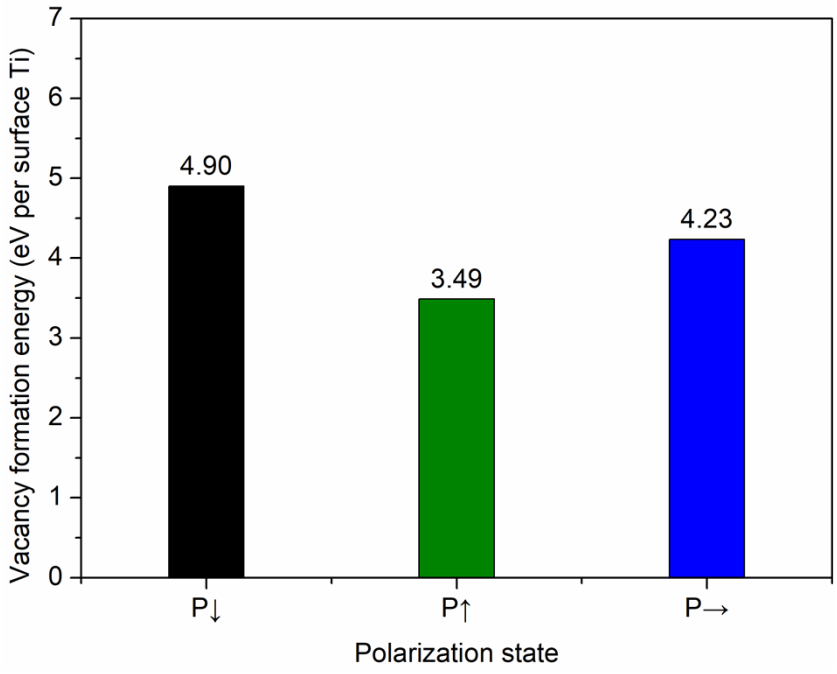

Figure S5 Formation energies of a Ti vacancy on BTO surface with hydrogen absorption under varied polarization states.

References:

1 G. Kresse and J. Furthmüller, *Phys. Rev. B*, 1996, **54**, 11169–11186.

2 J. P. Perdew, K. Burke and M. Ernzerhof, *Phys. Rev. Lett.*, 1996, **77**, 3865–3868.

3 G. Kresse and D. Joubert, *Phys. Rev. B*, 1999, **59**, 1758–1775.

4 P. E. Blöchl, *Phys. Rev. B*, 1994, **50**, 17953–17979.

5 S. Grimme, J. Antony, S. Ehrlich and H. Krieg, *J. Chem. Phys.*, 2010, **132**, 154104.

6 H. J. Monkhorst and J. D. Pack, *Phys. Rev. B*, 1976, **13**, 5188–5192.

7 R. D. King-Smith and D. Vanderbilt, *Phys. Rev. B*, 1993, **47**, 1651–1654.

8 Y. Watanabe, *Sci. Rep.*, 2021, **11**, 2155.

9 Y. Watanabe, *Phys. Rev. Mater.*, 2020, **4**, 104405.

10 S. L. Dudarev, G. A. Botton, S. Y. Savrasov, C. J. Humphreys and A. P. Sutton, *Phys. Rev. B*, 1998, **57**, 1505–1509.

11 A. A. Peterson, F. Abild-Pedersen, F. Studt, J. Rossmeisl and J. K. Nørskov, *Energy Environ. Sci.*, 2010, **3**, 1311–1315.

12 J. K. Nørskov, J. Rossmeisl, A. Logadottir, L. Lindqvist, J. R. Kitchin, T. Bligaard and H. Jónsson, *J. Phys. Chem. B*, 2004, **108**, 17886–17892.

13 H. Prats and K. Chan, *Phys. Chem. Chem. Phys.*, 2021, **23**, 27150–27158.

14 R. Kronberg, M. Hakala, N. Holmberg and K. Laasonen, *Phys. Chem. Chem. Phys.*, 2017, **19**, 16231–16241.

15 V. Wang, N. Xu, J.-C. Liu, G. Tang and W.-T. Geng, *Comput. Phys. Commun.*, 2021, **267**, 108033.

16 P. Abbasi, M. R. Barone, M. de la Paz Cruz-Jáuregui, D. Valdespino-Padilla, H. Paik, T. Kim, L. Kornblum, D. G. Schlom, T. A. Pascal and D. P. Fenning, *Nano Lett.*, 2022, **22**, 4276–4284.

17 W. Zhai, Y. Ma, D. Chen, J. C. Ho, Z. Dai and Y. Qu, *InfoMat*, 2022, **4**, e12357.

18 A. M. Patel, J. K. Nørskov, K. A. Persson and J. H. Montoya, *Phys. Chem. Chem. Phys.*, 2019, **21**, 25323–25327.

19 A. K. Singh, L. Zhou, A. Shinde, S. K. Suram, J. H. Montoya, D. Winston, J. M. Gregoire and K. A. Persson, *Chem. Mater.*, 2017, **29**, 10159–10167.

20 S. P. Ong, W. D. Richards, A. Jain, G. Hautier, M. Kocher, S. Cholia, D. Gunter, V. L. Chevrier, K. A. Persson and G. Ceder, *Comput. Mater. Sci.*, 2013, **68**, 314–319.

21 N. Artrith, W. Sailuam, S. Limpijumnong and A. M. Kolpak, *Phys. Chem. Chem. Phys.*, 2016, **18**, 29561–29570.

22 C. G. Van de Walle and J. Neugebauer, *J. Appl. Phys.*, 2004, **95**, 3851–3879.